ARCHITECTURAL RESEARCH, Vol. 3, No. 1 (2001), pp. 45-52

Structural Behaviors for Pressurized Fabric Leaning Arches

Jae Yeol Kim
School of architecture, Sungkyunkwan University, Suwon, Korea

Abstract

In this paper, a pressurized single vertical arch and a pressurized leaning arch composed of flexible fabric material are considered. These arches have also been considered as a possible support structure for the tent-like structures. Two different boundary conditions are considered in leaning arches with fixed bases and pinned bases. The behaviors of the leaning arches are investigated for two tilt angles as 15, 30 . For each angle, two loading conditions are considered as uniformly distributed load and wind loads. The F.E.M. is used through the all analysis procedures. For the results, load-deflection relationships, buckling modes, differences between two boundary conditions and deformed configurations are discussed.

Keywords : pressurized arch, tent-like structures, FE analysis, nonlinear analysis

1. INTRODUCTION

The tent-like structures will be used for many purposes including maintenance shelters, aircraft hangars, and medical stations. One of the possible support structures being considered is the air-inflatable arch. In order to facilitate easy erection the support structure of the tent-like structures is to be inflatable. Also, the support structure of the tent-like structures is to be lightweight and will most likely be constructed of a thin, woven or braided fabric, with an internal bladder to hold the air within.

Sanders and Liepins[1] discussed the behavior of a circular membrane subjected to an internal pressure. They derived membrane equations for the pressurized toroid using nonlinear membrane theory. However, these results are only valid for very thin shells where bending can be neglected. Tielking, et al. [2] extended Sanders and Liepins' theory for toroidal membranes further to account for the nonlinearity of the membrane solutions near the apex. The authors used a modified linear theory, which is based on the non-linear theory but linearized by neglecting the meridional stresses effect on the deformation. When studying wind load on a tent structure, Krainski[3] used a stepped distribution to represent a nonlinear wind distribution with pressure on the windward face and suction at the top and leeward face. Hou [4] used a non-uniform pressure, which varied from a pressure at the ground of the windward face to zero at the apex to a suction at the ground of the leeward face. In this paper, a pressurized single vertical arch and a pressurized leaning arch composed of flexible fabric material are considered. Fixed boundary is applied to vertical arch and two different boundary conditions are considered in leaning arches with fixed bases and pinned bases. The behaviors of the leaning arches are investigated for two tilt angles as 15 and 30. For each case, two loading conditions as uniformly distributed load and wind load are considered.

For each analysis, a shell element is used. The formulation procedures are omitted in this paper. The external loads are increased on the structure until one of the following situations occurs:

1) A bifurcation point is reached on the load-frequency graph

2) A limit point is reached on the load-frequency graph

3) The analysis stops because the incremental load step is too small. This is characteristic of local buckling on the arches.

If the analysis is stopped due to a bifurcation or limit point instability, the final load is referred to as the buckling load. If the analysis stops due to the solution diverging, then the failure is due to local buckling or wrinkling.

A bifurcation point is characterized by the load-frequency curve passing through a frequency of zero with a non-zero slope. A limit point is characterized by the load-frequency curve passing through a frequency of zero with a zero slope.

The arch material is assumed to be a linearly elastic, isotropic material with a modulus of elasticity of 7GPa and Poissons ratio of 0.3. Analyses of this type often neglect the self-weight of the structures; however, the structure under consideration is very large. Because of its size, the self-weight of the structure may be significant; therefore, it is included in the analysis. A density of 1440kg/m^3 is used. These values are representative of a lightweight woven fabric such as Kevlar or nylon.

2. ANALYSIS MODEL

The shape forms parabolic and the equation is as follow.

$$z(x) = H - (H/V^2)\, x^2 \qquad (1)$$

Here, for the base with 15 degree tilt angle θ shown in Fig.1(c), height H=16.42m and base width V=8.80m,

This work was supported partially by the Brain Korea 21 Project

cross-sectional radius r=0.4m and thickness t=0.25mm are imposed. And for the 30 degree tilt angle θ, height H=14.72 m and base width V=17.0 m are given.

The tilt angle is increased, the height of the leaning arches decreases and the base width increases. The geometrical shape is shown in Fig.1.

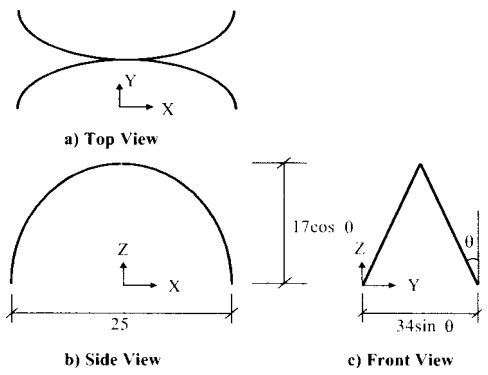

Fig.1. Geometrical shape of arch(unit:m)

The finite element mesh used in this analysis is created using Mathematica (Wolfram, 1993). A program that can create a generic mesh for any profile, tilt angle, or number of elements is desired. The process governing the position of any node on the surface of a vertical arch is as follows:

$$s_i = \frac{i \cdot s_0}{n} \tag{2}$$

$$s_0 = \int_0^{x_0} \sqrt{1 + z'(x)^2}\, dx \tag{3}$$

$$z_i = z(x_i) \tag{4}$$

$$\sin\gamma_i = \frac{z'(x_i)}{\sqrt{1 + z'(x_i)^2}} \tag{5}$$

$$\cos\gamma_i = \frac{1}{\sqrt{1 + z'(x_i)^2}} \tag{6}$$

$$\phi_j = \frac{j}{m} 2\pi \tag{7}$$

$$x_{ij} = x_i + r \cdot \sin\gamma_i \cdot \cos\phi_j \tag{8}$$

$$y_{ij} = r \cdot \sin\phi_j \tag{9}$$

$$z_{ij} = z_i + r \cdot \cos\gamma_i \cdot \cos\phi_j \tag{10}$$

where

n : the number of divisions along the arc length of the arch

i: the i^{th} division along the arc length of the arch $(0 \le i \le n)$

s_i : the arc length to the i^{th} point on the arch

s_0 : the arc length of the arch

$z(x)$:the function defining the shape of the arch in the vertical plane

x_0 : the first positive root of $z(x)$

x_i : the x coordinate of the i^{th} point on the arch and is the first positive root of $\int_0^{x_i} \sqrt{1 + z'(x)^2}\, dx - s_i = 0$

r : the radius of the cross section

γ : the angle between the plane of a cross section and the vertical axis

ϕ : the angle around the cross section $(0 \le \phi \le 2\pi)$

m : the number of divisions around the cross section

j : the j^{th} division around the cross section $(0 \le j \le m)$

x_{ij}, y_{ij}, and z_{ij} : the x, y, and z coordinates of any point on a vertical arch

An arch that is created using the equations above can be rotated by an angle θ from the vertical plane into a tilted position using the following transformations:

$$\psi = \tan^{-1}\left(\frac{y_{ij}}{z_{ij}}\right) \tag{11}$$

$$X_{ij} = x_{ij} \tag{12}$$

$$Y_{ij} = \sqrt{y_{ij}^2 + z_{ij}^2}\cos(\psi - \theta) \tag{13}$$

$$Z_{ij} = \sqrt{y_{ij}^2 + z_{ij}^2}\sin(\psi - \theta) \tag{14}$$

where

X_{ij}, Y_{ij}, and Z_{ij} : the coordinates of a leaning arch

ψ : the angle between the vertical XZ plane and any point on a vertical arch

θ: the tilt angle from the vertical

A second, leaning arch can be created by finding $Y_{ij\,max}$ for the tilted arch and then copying the original arch across the x-z plane at $y = Y_{ij\,max}$. The new y-coordinate ($Y_{ij\,new}$) becomes:

$$Y_{ij\,new} = 2Y_{ij\,max} - Y_{ij} \tag{15}$$

3. APPLYING LOADS

For every analysis, prior to the application of external loads, internal pressure of 500kPa is applied. At the final internal pressure, the arch deflects 5.87cm upwards at the apex. For further analysis of external loads, the deflection is reported as the displacement from the equilibrium position of the pressurized arch.

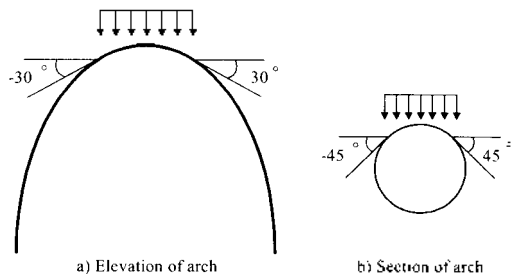

Fig.2. Arch Model subjected to uniformly distributed load

The uniformly distributed snow load is applied as shown in Fig.2. In this case, since the load is vertical and symmetric, only the deflections in the Z-direction at the apex are monitored.

Below equations are introduced as a numerical wind load.

- Case 1 (smooth) :

$$k(\theta) = -0.804 + 0.140\cos\theta + 1.380\cos 2\theta + 0.490\cos 3\theta - 0.318\cos 4\theta \quad (17)$$

- Case 2 (rough) :

$$k(\theta) = -0.258 - 0.488\cos\theta + 0.476\cos 2\theta + 0.328\cos 3\theta + 0.10\cos 4\theta \quad (18)$$

- Case 3 (beyer) :

$$k(\theta) = -0.655 - 0.28\cos\theta + 1.115\cos 2\theta + 0.40\cos 3\theta - 0.113\cos 4\theta - 1.027\cos 5\theta \quad (19)$$

- Case 4 (dischinger) :

$$k(\theta) = 0.75\cos\theta + 0.15\cos 3\theta \quad (20)$$

- Case 5 (girkmann) :

$$k(\theta) = -0.526 + 0.253\cos\theta + 0.95\cos 2\theta + 0.462\cos 3\theta - 0.189\cos 4\theta \quad (21)$$

- Case 6 (cosine) :

$$k(\theta) = \cos\theta \quad (22)$$

These equations lend themselves to finite element analysis where the wind pressure can be determined numerically for any length along an arch. Fig.3 shows the wind distribution as a function of coordinates x by using these equations. Case 1 and 2 are presented by Soar[5] from wind tunnel test and Case 3, Case 4 and Case 5 are presented by engineer who denoted in parenthesis.

4. VERTICAL ARCH SUBJECTED TO SNOW LOADS AND WIND LOADS

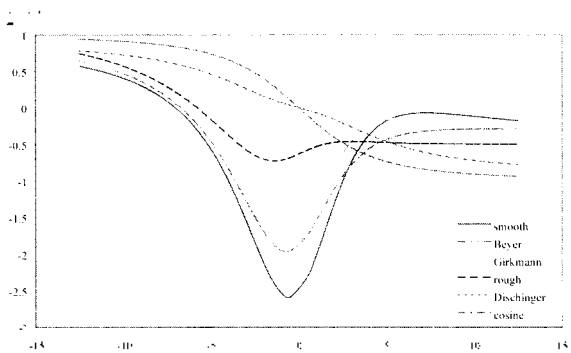

Fig.3. Wind distributions as a function of x

The load-deflection and load-frequency curves for snow loads are shown in Fig.4 and 5, respectively. The load deflection curve is slightly softening. In the load-frequency plot, the solid line is the first vibration frequency, the dashed line is the second frequency, and the dash-dot line is the third vibration frequency. The frequencies decrease as the load is increased. A view of the deflected shape at the buckling load in the X-Z plane is shown in Fig.6. It is known that bifurcation buckling was occurred(Fig.5).

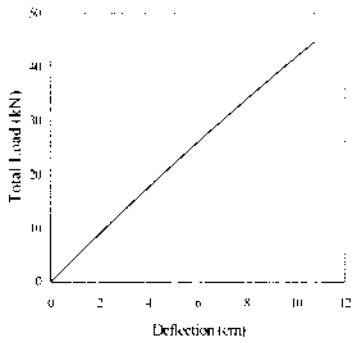

Fig.4. Total load vs. deflection

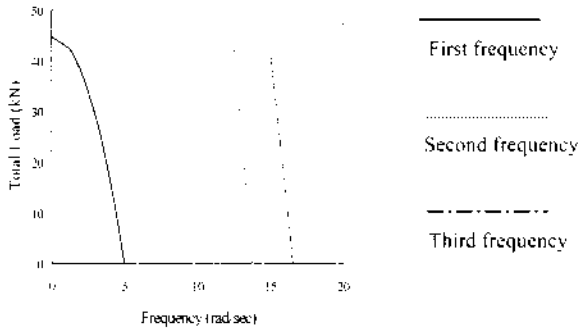

Fig.5. Total load vs. frequencies

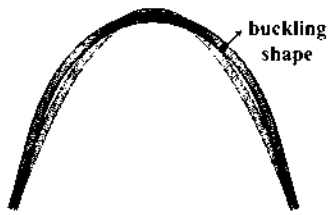

Fig.6. Deflected shape

For the wind loads, it can be proved from the results that Case 4 and Case 6 give results that are quite different from the other four distributions. These two pressure distributions give small vertical deflections ; however, the lateral deflections are very large. The large lateral deflections are due to the fact that both distributions have only pressure on the windward side of the arch and only suction on the leeward face of the arch. These two distributions are very simple models of wind pressure ; however, it appears that they are not realistic when compared to the results of pressure distributions which are obtained from wind tunnel testing.

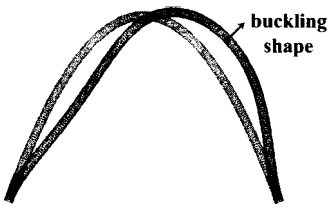

Fig.7. Deflected shape of single arch for rough wind distribution

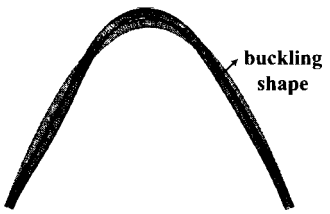

Fig.8. Deflected shape of single arch for smooth wind distribution

5. LEANING ARCH SUBJECTED TO SNOW LOADS

5.1 15 degree tilt angle with fixed boundary

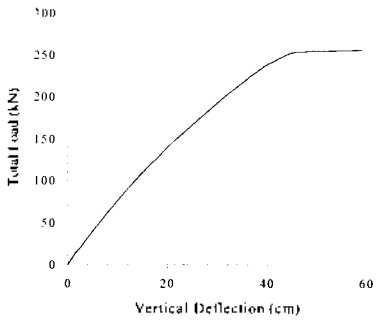

Fig.9. Total load vs. deflection

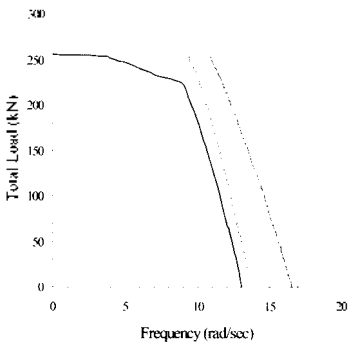

Fig.10. Total load vs. frequencies

The load is increased until the first vibration frequency becomes zero, which occurs at a load of 253kN(56.9kips). At the final load, the apex of each arch deflects downward 45.5cm(17.9in.) from the pressurized equilibrium position, the second frequency is 9.35rad/sec, and the third frequency is 10.82rad/sec. The load-deflection and load-frequency curves are shown in Fig.9 and 10, respectively. The side view of the displaced shape at the buckling load is shown in Fig.11.

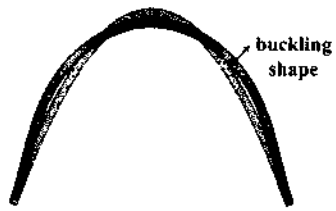

Fig.11. Deflected shape

5..2 30 degree tilt angle with fixed boundary

The load-deflection curve is shown in Fig.12, the load-frequency curve is shown in Fig.13, the side view of the deflected shape at the final load is shown in Fig.14.

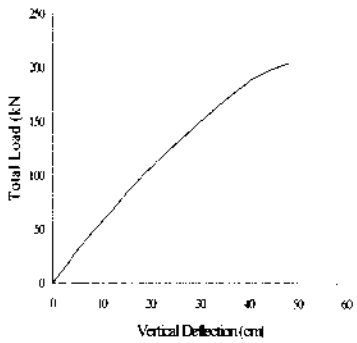

Fig.12. Total load vs. deflection

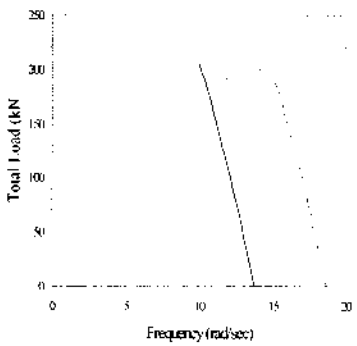

Fig.13. Total load vs. frequencies

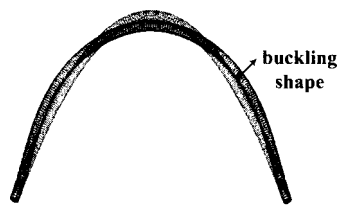

Fig.14. Deflected shape

5.3 15 degree tilt angle with pinned boundary

These views of the first three vibration modes are shown

in Fig.15 through 17. Since the first frequency is zero, the first mode shape is the buckled configuration.

Fig.15. Buckling mode (twist)

Fig.16. Second vibration mode (longitudinal sway)

Fig.17. Third vibration mode (side sway)

5.4 30 degree tilt angle with pinned boundary

These views of the first three vibration modes are shown in Fig.18 through Fig.20. Since the first frequency is zero, the first mode shape is the buckled configuration.

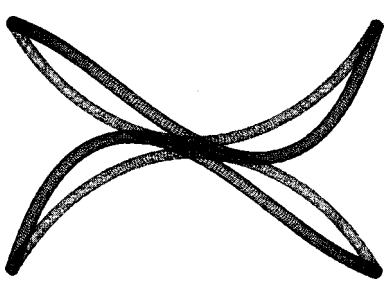

Fig.18. Buckling mode (twist)

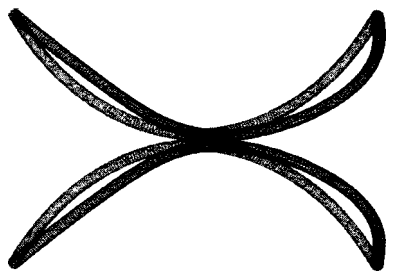

Fig.19. Second vibration mode (longitudinal sway)

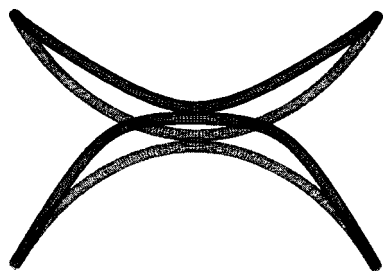

Fig.20. Third vibration mode (side sway)

6. LEANING ARCH SUBJECTED TO WIND LOADS

6.1 15 degree tilt angle with fixed boundary

Case 2(rough) in section 2.4.4 is applied as a wind load. The wind load is increased until the pressure is 11.31kPa(236.2psf).

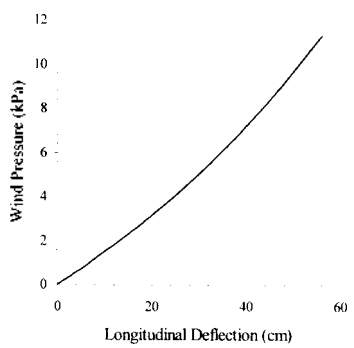

Fig.21. Wind pressure vs. longitudinal deflection

The analysis is stopped at this load because the wind pressure is excessive and the behavior of the structure can be determined from the loading sequence ; therefore, larger loads do not need to be applied.

At this pressure the longitudinal deflection of the arches is 56.0cm and the vertical deflection is 4.13cm. The pressure- deflection curves are shown in Fig.21 and 22. At the final load, the first vibration frequency is 14.0rad/sec, the second frequency is 14.4rad/sec, and the third frequency is 18.6rad/sec. The first vibration mode of the arches is shown in Fig.23.

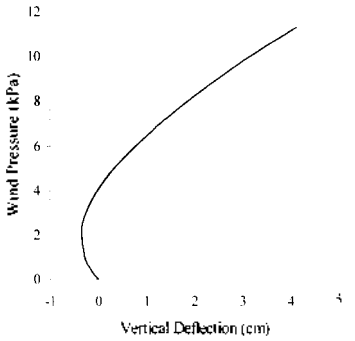

Fig.22. Wind pressure vs. vertical deflection

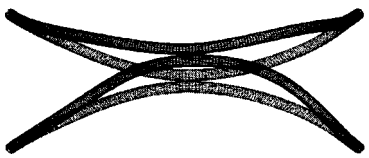

Fig.23. First vibration mode (side sway)

6.2 30 degree tilt angle with fixed boundary

Fig.24 shows the pressure-longitudinal deflection curve. Fig.25 shows the pressure-frequency curves.

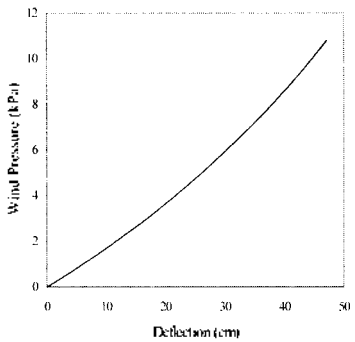

Fig.24. Wind pressure vs. longitudinal deflection

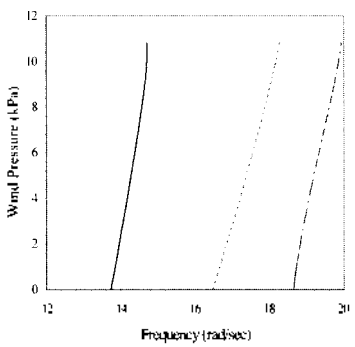

Fig.25. Wind pressure vs. frequencies

6.3 15 degree tilt angle with pinned boundary

The pressure-deflection curves are shown in Fig.26 and 27. At the final load, the first vibration frequency is 9.07rad/sec, the second frequency is 9.95rad/sec, and the third frequency is 11.62rad/sec. The pressure-frequency curves for the first and second vibration modes cross at a pressure of approximately 2.8kPa. The first vibration mode of the arch is shown in Fig.28.

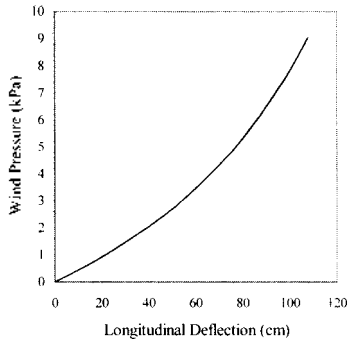

Fig.26. Wind pressure vs. longitudinal deflection

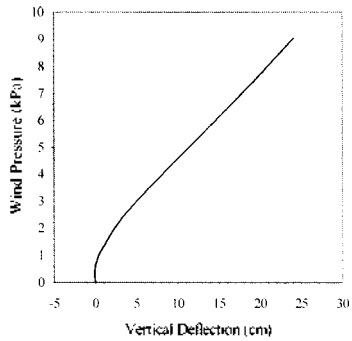

Fig.27. Wind pressure vs. vertical deflection

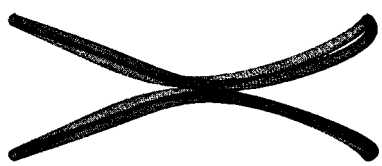

Fig.28. First vibration mode (longitudinal sway)

6.4 30 degree tilt angle with pinned boundary

The pressure-deflection curves are shown in Fig.29, where the solid line gives the longitudinal deflection and the dashed line gives the vertical deflection. Finally, the first vibration mode of the arch is shown in Fig.30.

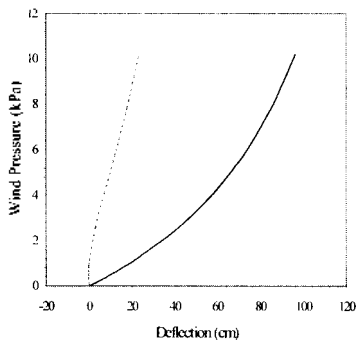

Fig.29. Wind pressure vs. deflection

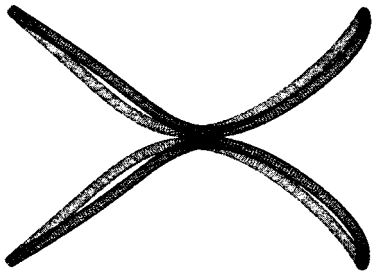

Fig.30. First vibration mode (longitudinal sway)

7. RESULTS SUMMARY FOR LEANING ARCHES

A summary of the results for the leaning arches tilted at 15° and 30° for fixed and pinned bases and for three load distributions is shown in Fig.31 to Fig.36. In Figures, a first frequency of zero signifies that the arches buckled at the load specified by "final load."

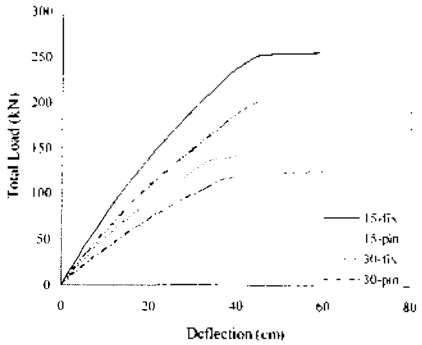

Fig.31. Total load vs. vertical deflection for leaning arches with full snow

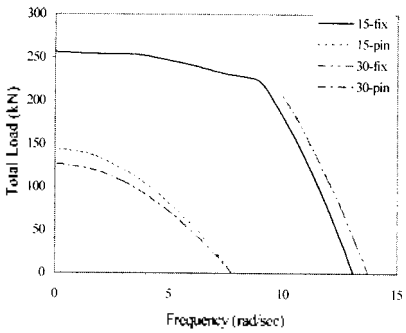

Fig.32. Total load vs. first frequency for leaning arches with full snow

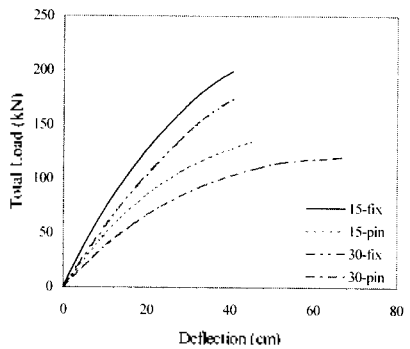

Fig.33. Total load vs. vertical deflection for leaning arches with half snow

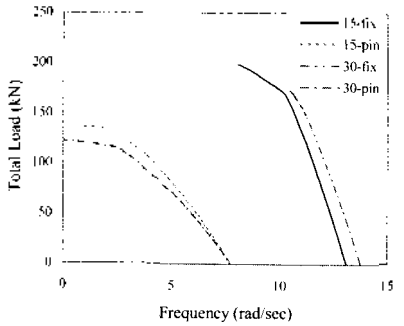

Fig.34. Total load vs. first frequency for leaning arches with half snow

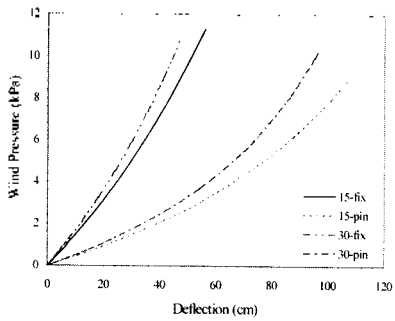

Fig.35. Wind pressure vs. longitudinal deflection for leaning arches with wind

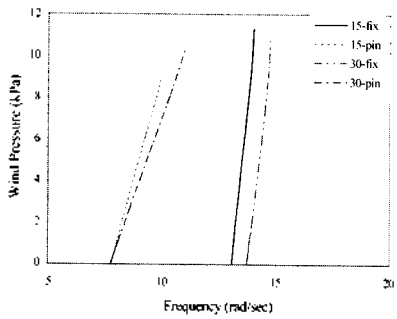

Fig.36. Wind pressure vs. first frequency for leaning arches with wind

Cross-sectional deformations were taken into account during the analyses presented in this paper. As expected, cross-sectional deformations were significant.

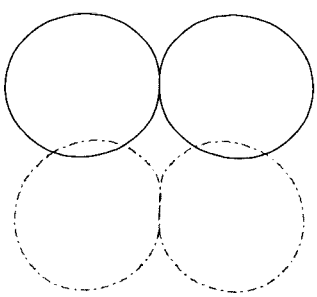

Fig.37. Displaced cross-section at apex under full snow load

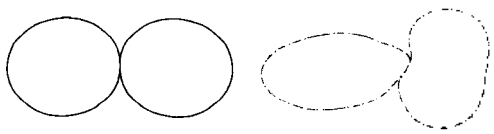

Fig.38. Displaced cross-section at apex during side sway vibration mode

Two typical displaced cross sections are shown in Fig.37 and 38. Fig.37 shows the displaced cross section at the apex for arches under a uniformly distributed load of 143kN, with pinned bases, and tilted at 15. It can be seen that the arches come into further contact with each other, causing the once circular cross section to become oval-shaped. The cross-sectional deformation of the toroid is nearly identical with that of toroidal finite element model presented by Sanders and Liepins(1963).; however, the finite element model developed in this paper(Fig.37) moves upwards at the apex. This upward movement is most likely due to the fixed ends of the model. Fig.39 shows the displaced shape of the cross section at the apex for the side sway vibration mode. This figure is for leaning arches with pinned bases, tilted at 15, and with only an internal pressure of 500kPa. This figure shows how the cross section can change as the arches move.

8. CONCLUSIONS

Various structural behaviors for the arches are investigated. Bifurcation buckling is occurred in the vertical arch(Fig.5). Limit buckling occurs for uniformly distributed load on the leaning arches with pinned bases tilted at both 15 and 30 ; however, buckling only occurred for uniformly distributed load on the leaning arches with fixed bases tilted at 15(Fig.33). For wind load cases, no buckling occurs in the range of loads considered(Fig.37). The boundary conditions of the arches have a significant impact on the behavior of the leaning arches. Fixed bases cause the structure to be much stiffer, stronger, and more stable. The vibration frequencies are higher for fixed bases when compared to the arches with pinned bases. The deflections are also smaller for the arches with fixed bases.

The tilt angle has a less significant impact on the behavior of the leaning arches. For the uniformly distributed load, the arches tilted at 30 have larger vertical deflections than the arches tilted at 15 ; however, the arches with a 15 tilt angle have larger longitudinal deflections than the arches tilted at 30. From the vibration modes, it can be shown that the first vibration mode for the arches with pinned bases is often a twisting mode ; however, the first vibration mode for the arches with fixed bases is a side sway mode. This difference in vibration mode shows that the lack of restraint at the pinned bases causes the pinned arches to be much weaker in twisting than the fixed arches. Wrinkling of the arches occurred near the final load for many of the load cases. This may suggest that the wrinkling load has been passed. The finite element model, however, did not develop fold lines like those that might be expected when a thin fabric loses its tensile prestress. The leaning arch module is a very efficient structure. A single arch with fixed bases buckles at a total load of 45kN, but a pair of leaning arches tilted at 15 with fixed bases buckles at 253kN. Adding a second arch increases the load carrying capacity of the structure by 550%. Only two types of loads have been considered to act on the structure. The two loads studied are the most common ; however, other load types should be considered, such as loads perpendicular to the length of the arches, or loads which act at an oblique angle to the arches. And, this paper is dealt with the linearly elastic, isotropic, and homogeneous material, however, different properties in various directions, which may significantly impact the behaviors of the structures should be considered. If tents are designed using leaning arches, the leaning arch structure should be optimized to obtain a shape, tilt angle, cross section, and internal pressure which has large critical loads, small deflections, and a low weight.

REFERENCES

1. Sanders, J .L. and Liepins, A. A., Toroidal Membrane Under Internal Pressure, *AIAA Journal*, Vol. 1, No. 9, pp. 2105-2110, 1963
2. Tielking, J. T., McIvor, I. K. and Clark, S.K., Modified Linear Membrane Theory for the Pressurized Toroid. *Journal of Applied Mechanics*, Vol. 38, No. 2, pp. 418-422 , 1971
3. Krainski, W. J, Investigation of Alternative Framing Arrangements Using Pressure-Stabilized Beams for Battalion Aid Station Support, *Technical Report TR-88-071*, U. S. Army Natick Research and Development Laboratories, Natick, MA., 1988
4. Hou, A, *Analysis of the Deflections, Vibrations, and Stability of Leaning Arches*, Masters Thesis, Virginia Polytechnic Institute and State University, Blacksburg, VA., 1996
5. Soare, M., *Application of Finite Difference Equations to Shell Analysis*, Pergamon Press, New York, NY., 1967
6. Dietz, A. E., Proffitt, R. B., Chabot, R. S., Moak, E.L. and Monego, C.J., "Wind Tunnel Tests and Analysis for Ground-Mounted Air-Supported Structures," *Technical Report TR-70-7-GP*, U. S. Army Natick Research and Development Laboratories, Natick, MA., 1969
7. Hibbitt, Karlsson, and Sorenson Inc., *ABAQUS*, Pawtucket, RI., 1994
8. Kawabata, M. and Ishii, K., Study on Structural Characteristics of Air-Inflated Beam Structures, *International Association for Shell and Spatial Structures Symposium*, April, 24-28, Atlanta, GA., 1994
9. Wolfram, S., *Mathematica: A System of Doing Mathematics by Computer*, Wolfram Research, Inc., Champaign, IL., 1991